Adsorption (2006) 12:45–54
DOI 10.1007/s10450-006-0137-0

Ethane adsorption in slit-shaped micropores: influence of molecule orientation on adsorption capacity

G. Calleja · B. Coto · A. Pinar · A. M. Morales-Cas

Received: 30 December 2005 / Revised: 6 June 2006 / Accepted: 23 June 2006

Abstract Adsorption of ethane in a slit shaped micropore system has been studied by Monte Carlo molecular simulation by considering this hydrocarbon as a two interacting sites molecule. Ethane adsorption in pore sizes from 0.41 to 1.66 nm was simulated at 303 K. Microscopic characteristics of the adsorbed phase have been studied for pores of different size, comparing two density profiles: the molecule centre of mass profile and the molecular interaction site profile. Averaged angle distribution of molecule positions with respect to the slit plane across the pore width has been also obtained by simulation. These results were related to ethane molecule packing efficiency, which is also related to the adsorption capacity in terms of the adsorbed phase density. Packing efficiency presents an oscillation shape as the result of the adsorbate disorder inside the pore.

Pressure influence on the adsorption has been studied by following pore filling by simulation. When pore condensation takes place and for pressures above condensation, fluid-fluid interactions are determinant in molecule disorder observed between the two adsorbed layers.

Keywords Activated carbon · Slit pore model · Molecular simulation · Monte Carlo simulation · Ethane

G. Calleja (✉) · B. Coto · A. Pinar · A. M. Morales-Cas
Department of Chemical and Environmental Technology, ESCET, Rey Juan Carlos University, c/ Tulipán s/n 28933 Móstoles, Madrid (Spain)
e-mail: guillermo.calleja@urjc.es

1 Introduction

Microporous carbons are among the most used adsorbents for liquid and gas streams. Characteristics of adsorbed light hydrocarbons in microporous carbons have been widely studied (Mota, 1999; Liu and Monson, 2005). As the second component of natural gas, ethane is a compound of special interest for the energy industry (Gall and Sanders, 2002) due to the increasing development of natural gas driven automobile devices. These applications require a high efficiency in natural gas storage, being adsorption in porous materials one of the most attractive alternatives, as suggested in several studies (Lozano-Castelló, 2002).

Adsorption selectivity of methane and ethane is highly influenced by the presence of heavier hydrocarbons such as propane and butane. The adsorption behaviour of ethane and its mixtures with various light hydrocarbons such as methane and propane in microporous carbons has been considered widely in recent years (Cracknell and Nicholoson, 1994; Zhou et al., 2005).

Besides these experimental studies, advanced computational methods such as Monte Carlo or Density Functional Theory have been applied to adsorption studies of several adsorbate-adsorbent systems, pointing up the applications in textural characterization of porous media based on adsorption data of several molecules, like N_2, CO_2, Ar, (Yan and Yang, 2005), methane and ethane at sub or supercritical temperature (Davies and Seaton, 2000). In addition, ethane can be

considered as a linear molecule model, and its non-polar nature allows studying the structural dependency related to the pore geometry in carbon porous materials. The most common pore model used to describe microporous carbons is the slit-shape model, considering the independent pore approach, where both connectivity and edge influence are not taken into account.

There are some published studies on the structural characteristics of adsorbed linear molecules in slit-like pores (Vishnyakov et al., 1996; Klochko, 1999) and their dependency on pore size, temperature, and chemical potential. More recently, Do and Do (2004) related these structural characteristics to the packing efficiency of the adsorbed molecule, for ethylene below its critical temperature. Packing efficiency of an adsorbate has an influence on the adsorption isotherm shape, which could exhibit a gradual rise or a steep jump for pores differing slightly in size (Suzuki et al., 1997). In addition, this efficiency also influences the relation between adsorption capacity and pore size (Olivier, 1998; Do and Do, 2004). If adsorption capacity is considered as the maximum adsorbate density reached in the isotherm, its variation with pore size presents an oscillating shape (Olivier, 1998; Do and Do, 2004; Nguyen et al., 2002).

In this context, this work is founded on the structural properties of ethane in slit-like pores of a carbon at a temperature closed to the critical point, considering pressure effects and emphasizing the effect of small variations in pore size within the microporous range.

2 Potential model

Ethane molecules were modelled as two 12-6 Lennard-Jones (LJ) sites separated 0.154 nm with interaction parameter values $\sigma_{ff} = 0.375$ nm and $\varepsilon_{ff}/k_B = 98$ K (Martin and Siepmann, 1998), being k_B the Boltzmann constant. Adsorbent pores were simulated as two parallel walls dimensioned L^2. Periodic boundary conditions were imposed along x and y directions since the solid walls were placed confining the system in z direction. The so-called 10-4 potential (W.A. Steele, 1974) was used to describe the interaction between each LJ site molecule and the solid carbon wall; it is given by:

$$U_{sf}^{LJ\,i}(z) = 2\pi\rho_s\sigma_{sf}^2\varepsilon_{sf} \times \left[\frac{2}{5}\left(\frac{\sigma_{sf}}{z}\right)^{10} - \sum_{i=0}^{2}\left(\frac{\sigma_{sf}}{z+id}\right)^{4}\right] \quad (1)$$

where U_{sf}^{LJi} is the potential interaction energy between the LJ i site, and the solid wall. Using this model each pore wall is composed of one stack of three graphitic layers equally spaced, being z the distance between the LJ i site and the nearest plane of the wall, $\rho_s = 38.2$ atom nm^{-2} the area density of carbon atoms in a graphitic plane and $d = 0.335$ nm the space between graphitic planes in each stack. Solid-fluid interaction parameters, σ_{sf} and ε_{sf}, were calculated using the Lorentz Berthelot combining rules with values of σ_{ff} and ε_{ff} given above and the LJ parameters $\sigma_{ss} = 0.340$ nm and $\varepsilon_{ss}/k_B = 28$ K.

The total potential energy of a molecule confined in the pore volume, U_T, is the result of fluid-fluid and solid-fluid contributions:

$$U_T = U_{ff} + U_{sf} \quad (2)$$

where U_{ff} is the potential energy between fluid molecules (interaction between the two sites within a molecule is not allowed), and U_{sf} the potential energy for one molecule due to the presence of each solid wall. This potential is given by:

$$U_{sf} = \sum_{i=1}^{2} U_{sf}^{LJ\,i}(z) + \sum_{i=1}^{2} U_{sf}^{LJ\,i}(H-z) \quad (3)$$

where H is the pore width, that is the distance connecting the centre of atom carbons in the first graphitic layer on each pore wall.

3 Simulation details

All simulations were carried out in a grand canonical ensemble using the Monte Carlo simulation method (GCMC), where chemical potential, volume and temperature are taken as independent thermodynamic variables (Allen and Tildesley, 1987). Chemical potential was related to pressure by means of the Soave-Redlich-Kwong equation of state (SRK) (Poling et al., 2001) for a specified pressure and temperature. The ideal gas was taken as reference state for chemical potential and it was calculated from its partition function (McQuarrie and Simon, 1997). Four kinds of molecule moves were attempted to construct the Markov chain of system configurations: creation, rotation, mass center displacement and deletion. In order to keep the microscopic detailed balance and avoid systematic errors, attempting

probabilities for centre of mass displacement, molecule rotation, creation and deletion were kept constant, regardless of the number of particles; in addition, it was imposed that attempting probabilities for creation and deletion were equal (Frenkel and Smit, 2002). The probabilities (for acceptance) related to each type of move can be found elsewhere (Lachet, et al., 1997). In every simulation 10^7 configurations were generated; cut off distance was large enough (6σ) to avoid the use of long-range corrections, due to the difficulty of computing them in a non-homogeneous system (Duque and Vega, 2004).

From GCMC calculation, density profiles for molecule centre of mass and for interacting sites were obtained.

The density profiles, $\rho(z)$, were achieved computing the number of molecules (or LJ sites) in a differential volume $L^2\Delta z$, according to:

$$\rho(z) = \langle N(z)\rangle L^{-2}\Delta z^{-1} \tag{4}$$

where $\langle N(z)\rangle$ is the average number of the species considered, i.e. the molecule centre of mass, or the two interacting sites separately, contained in the differential volume. The pore volume was defined as the corresponding to a pore width value of :

$$d_p = H - \sigma_{ss} \tag{5}$$

to avoid the physical inconsistency of taking H as the pore width (Neimark and Ravikovitch, 1997).

In addition, wall-molecule angle distribution across the pore width was calculated. It was done averaging the molecule-wall angle in x and y directions for the same differential volume considered in density profile calculation:

$$\theta(z) = \arcsin\left(\frac{\langle \Delta z_{1,2}\rangle_z}{1}\right) \tag{6}$$

where $\theta(z)$ represents the average molecule-wall angle, $\Delta z_{1,2}$is the difference between the z-coordinates of sites 1 and 2 in a molecule, $\langle\rangle_z$ denotes that the average is taken inside the z-slice differential volume $\mathrm{L}^2\Delta z$, and l is the distance between sites.

The distribution functions so obtained provide a tool for a microscopic description of the adsorption phenomena.

4 Results and discussion

Adsorption data were simulated for ethane in a pressure range from 1 to 1000 kPa at a temperature of 303 K. Pore size was varied within the range from 0.41 to 1.66 nm, assuming no interacting cavities in the independent pore model.

4.1 Density profiles

For several pore sizes in the range 0.41 to 0.61 nm and different pressures, density profiles were obtained. Density values for the two interacting sites and the centre of mass profiles were plotted in reduced units, molecules per volume unit, ρ^*, being σ the length unit. They are shown together in the same plot to achieve a qualitatively description of the molecular orientation across the pore width (Fig. 1). The number of layers formed inside the pore width is accounted from the centre of mass profile. If in a given pore, or within a pore region, the molecule sites and centres of mass of ethane are mainly aligned within the z-slice, a coincidence of profiles is achieved, and the most common molecule orientation is parallel to the pore walls. The opposite situation is represented by the pair of profiles that do not exhibit peaks located in the same z-slice; in this case, centres of mass and interacting sites are aligned with Z axis and molecules are mainly vertical oriented to the pore walls.

Pore sizes plotted in Figure 1 are considered as representative of the evolution from one to two adsorbed layers. Figure 1(a) corresponds to a well defined layer inside the pore, since density profiles are coincident in the peak location; consequently centres of mass and interacting sites are aligned with respect to the pore wall. For a slight increase in pore width, from 0.41 to 0.49 nm (Fig. 1(b)), the situation changes: the site density profile exhibits two peaks and the centre of mass only one, which suggests a molecular reallocation with respect to the smaller pore size. This location must be related to an equal intensity in the interaction of each site and each pore wall within a pore size slightly wider than one molecular size. In addition, the peak density in the centre of mass profile diminishes, which is related to a decrease in adsorption capacity. For a larger pore size of 0.57 nm (Fig. 1(c)) this effect is more evident, observing a noticeable density peak decrease. Both site and centre of mass peaks become broader and site profile does not present a well-defined two peak shape. These

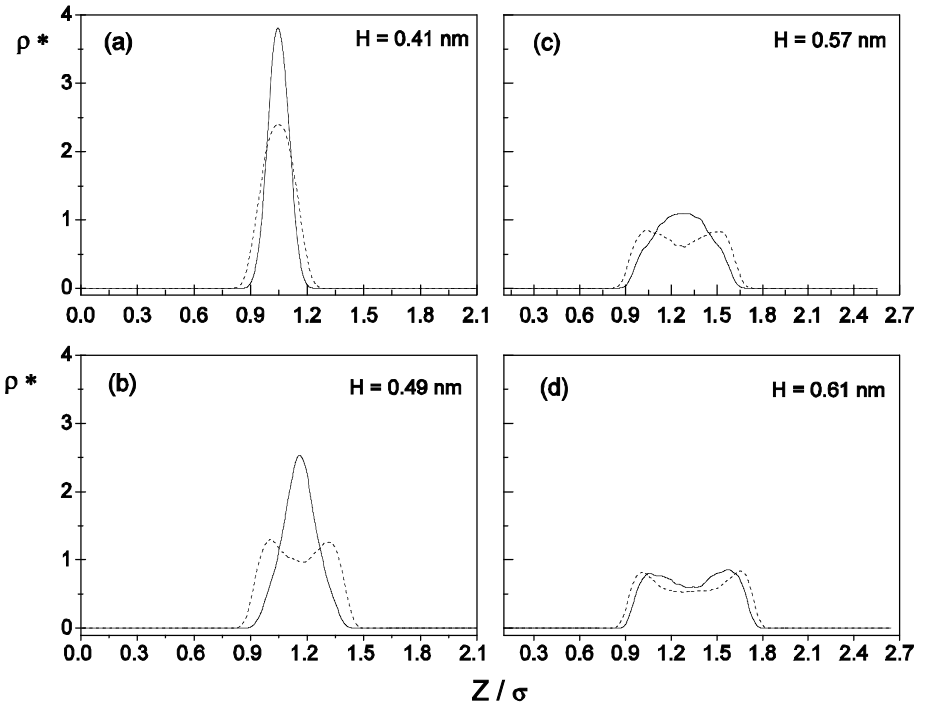

Fig. 1 Density profiles for interacting sites (dash line) and molecule centre of mass (solid line) for pores holding one adsorbate layer at saturation pressure (being H the pore width)

results are a qualitative observation of the increase in molecular disorder within this pore range. For the pore size of 0.61 nm (Fig. 1(d)) centre of mass and site profiles have a similar shape, showing a two peak profile, although not well-defined; it is only necessary a slight increase in pore width to hold two well defined adsorbate layers.

Representative density profiles matching the transition from two to three adsorbed layers are plotted in Fig. 2 (H from 0.65 to 1.06 nm). Differences between site and centre of mass density profiles within this pore range are now less pronounced than those within the first pore range commented (Fig. 1). However, still interesting differences can be appreciated.

Figure 2(a) (0.65 nm) corresponds to the smallest pore width that can hold two layers inside. Both site and centre of mass profiles change from those corresponding to the smaller pore size of 0.61 nm (Fig. 1(d)). A two peak profile is attained both for site and for centre of mass, which corresponds to a parallel orientation of molecules next to both pore walls. However, site profile exhibits a slight peak in the centre of the pore size, due to molecules that are not clearly arranged in the two layers next to the pore walls. As pore width increases up to 0.98 nm (Fig 2(c)) centre of mass and site profile peaks become more different, and the site profile exhibits two shoulders, which indicates a molecular reorganization inside the pore region close to the walls. Finally, for the largest pore size of 1.06 nm (Fig. 2(d)), a three peak profile is observed, both for the centre of mass and site profiles.

4.2 Molecule orientation

Details of molecule orientation from site and centre of mass density profiles are given by the angle profile analysis, which allows a quantitative description of the molecule orientation across the pore width. The results now presented correspond to the cases already discussed and shown in Figs. 1 and 2. The entire set of angle distribution represented in Fig. 3 shows the lowest angle values for those molecules close to the pore walls. The middle region of the pore width exhibits the highest angle value, in all cases being below 60°.

Thus, for the smallest pore size of 0.41 nm (Fig. 3(a)), angle value within the entire pore is below 20°, meaning that the preferential orientation is parallel to the pore wall, as commented previously.

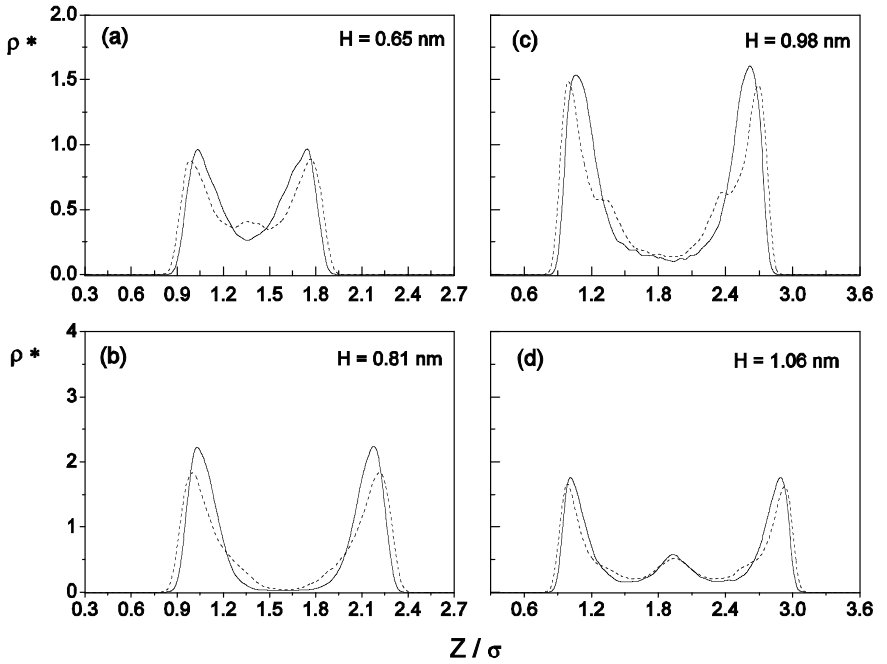

Fig. 2 Density profiles for interacting sites (dash line) and molecule centre of mass (solid line) for pores holding two or three adsorbate layers at saturation pressure (being H the pore width)

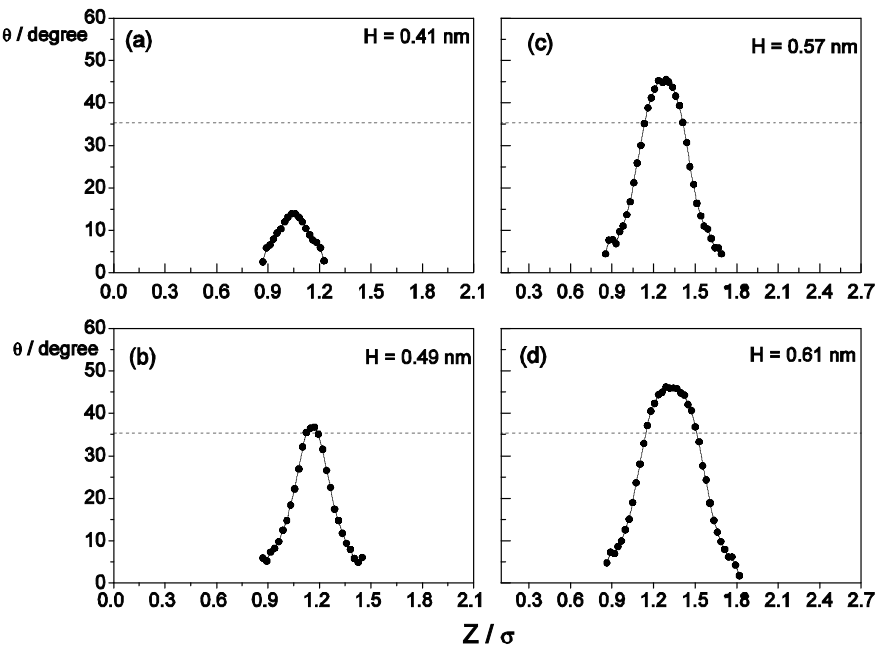

Fig. 3 Angle distributions of ethane molecules, across the pore width, for pores holding one adsorbate layer at saturation pressure. Dash line represents angle for freely rotating molecules

In the space close to the walls, θ diminish due to the alignment of molecules, being two sites adsorbed onto the same pore wall. Larger pore sizes like 0.49 nm (Fig. 3(c)), lead to the molecular relocation mentioned above, as a consequence of a disorder increase in the middle of the pore region, where θ is close to 45°. This tendency is more pronounced for the pore width of 0.57 nm (Fig. 3(c)), where θ reaches its maximum value, 45°, within the pore range. For the largest pore size of 0.61 nm (Fig. 3(d)), the angle profile shows a broad peak corresponding to $\theta = 45°$, being disorder orientation even more significant.

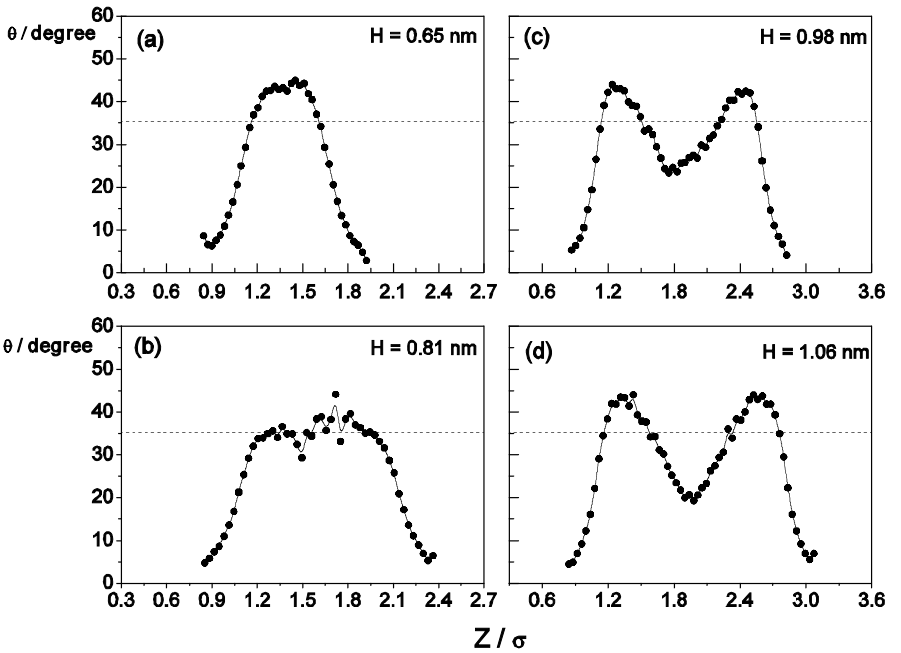

Fig. 4 Angle distributions of ethane molecules, across the pore width, for pores holding two and three adsorbate layers at saturation pressure. Dash line represents angle for freely rotating molecules

Molecule-angle distributions for the larger pore sizes, as plotted in Fig. 4, differ significantly from those shown in Fig. 3. There is now a noticeable data scattering for the middle pore region, as observed in Fig. 4(a) and Fig. 4(b); this is the result of the few molecules filling this pore region, as shown by the density profiles (Fig. 2(a) and 2(b)). For the pore size of 0.65 nm (Fig. 4(a)), molecules close to the pore walls have a vertical orientation, and the few that are located in the middle of the pore show an average angle of 45°. The pore size of 0.81 nm (Fig. 4(b)) presents angle values in the middle of the pore that correspond to freely rotating molecules. Figure 4 also shows that the molecule angles in the middle of the pore decrease with the pore size, indicating a decreasing number of molecules that are held in a random fashion. This tendency is more evident as the pore size increases (Fig. 4(c) and (d)). The molecular rearrangement in three layers, observed for the pore size of 1.06 nm (Fig. 4(d)), clearly shows the progressive molecular orientation along the pore width, having two zones of vertical orientation (θ about 45°) and three layers of a more parallel orientation, two closer to the pore walls, and the third one in the middle of the pore.

4.3 Adsorption isotherms

Figure 5 shows the adsorption isotherms of ethane obtained by molecular simulation in pores ranging from 0.41 to 1.66 nm, at 303 K. They are grouped in three intervals, according to the number of adsorbate layers formed, as discussed previously. The first group of isotherms, corresponding to the pore sizes ranging from 0.41 to 0.61 (Fig. 5(a)), shows a rapid condensation effect inside the pores in a low pressure range, where only one adsorbate layer is formed. The adsorption capacity, expressed by pore volume, decreases with pore width, within the pressure range approaching the saturation (100 kPa). For the second pore range studied, from 0.65 to 0.86 nm (Fig. 5(b)) all adsorption curves show a similar tendency in adsorption capacity, which is higher for the smaller pore sizes up to a pressure value around 50 kPa. Beyond this point, a reverse trend in adsorption capacity is observed. Priority of pore filling at low pressures corresponds to smaller pores, as expected. At higher pressures (beyond 50 kPa), pore filling involves larger pores that can hold a larger number of molecules, forming several adsorbate layers. Similar observations can be made for the largest pore size range studied, shown in Fig 5(c). So, as pore filling progresses, the contribution of smaller pore sizes becomes less significant to the total adsorption capacity. For the whole pore range studied, the wider the pore the higher the pressure corresponding to condensation.

Temperature selected for simulation (303 K) is close to the critical temperature of the bulk gas (Tc = 305 K). For a confined fluid critical temperature is below the

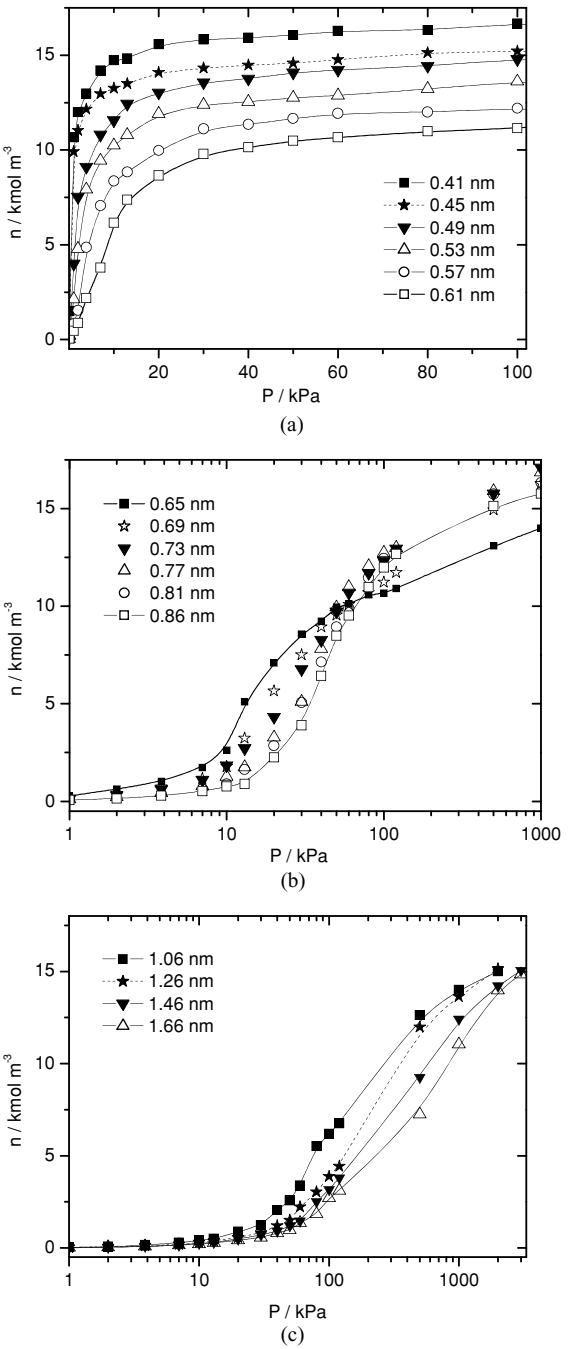

Fig. 5 Individual ethane adsorption isotherms for pore sizes holding one adsorbate layer (a), two adsorbate layers (b) and three adsorbate layers (c)

one corresponding to a bulk gas. The isotherm shape for a supercritical temperature does not exhibit a steep jump, but a gradual rise (Klochko et al., 1999), as it is observed for the entire isotherm set studied (Fig. 5).

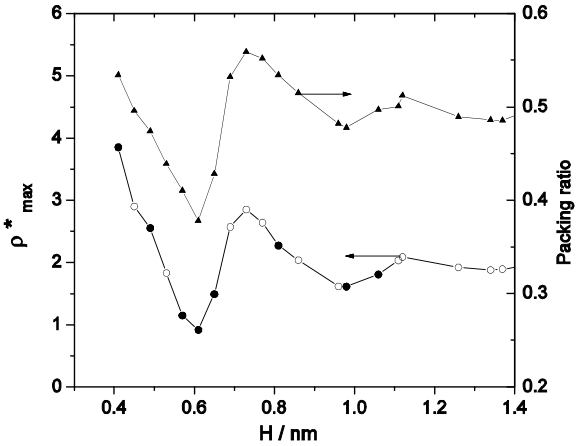

Fig. 6 Maximum adsorbate density (ν) and packing ratio (7) for several pore sizes at a pressure corresponding to saturation

Values of maximum density of ethane molecules corresponding to every isotherm are plotted vs. pore size in Figure 6. Previous studies have related packing efficiency with maximum molecular density in an adsorbing cavity for spherical and linear molecules (Suzuki and Gubbins, 1997; Do and Do, 2004). The oscillations observed for the maximum molecular density shown in Fig. 6 are in agreement with the corresponding oscillations in the packing ratio, also plotted in the same figure. Packing ratio values were calculated by dividing the volume of ethane molecules by the total pore volume completely filled. There is a density decrease with pore size for pores containing one adsorbate layer inside, in the pore range from 0.41 to 0.61 nm. As shown in Fig. 6, minimum density of molecules corresponds to 0.61 nm, which is the smallest pore size that holds two adsorbate layers inside. Thus in the transition from one to two layers, the change in packing efficiency does not correspond to a change in the number of adsorbed layers, but to a pore size just wider (H = 0.65 nm) than the one holding two adsorbate layers. This tendency suggests that the most efficient packing is related to the molecular orientation within the pore. Similar results were observed for subsequent layer transitions.

4.4 Pressure effect

To show the relation between pore filling mechanism and molecular orientation, some angle distributions across the pore width are plotted for several pressure values in Fig. 7. Complementary, the evolution of the centre of mass profile is shown. Selected pore

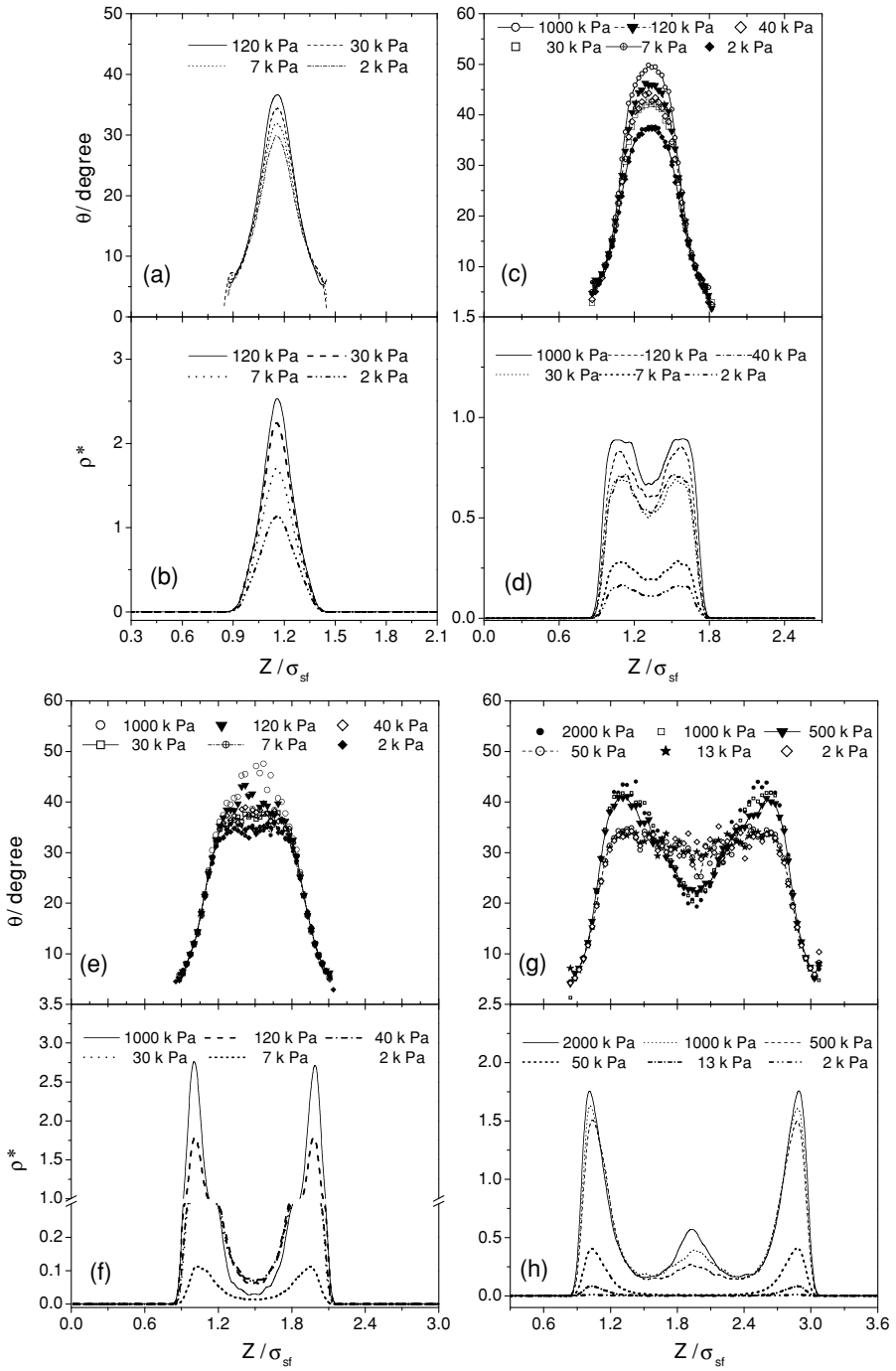

Fig. 7 Angle distributions and centre of mass profiles at various pressures for $H = 0.41$ nm (a–b), $H = 0.61$ nm (c–d), $H = 0.73$ nm (e–f), $H = 1.06$ nm (g–h). Lines are guide to eye.

sizes for these figures are those representatives of the one to two, and the two to three layer transitions (0.49; 0.61, 0.73 and 1.06 nm). It is observed that the major variation in the angle value with pressure occurs for molecules located in the middle of the pore width, where molecule orientation becomes more vertical to the pore wall. However, for those molecules close to the pore walls having a parallel orientation as

commented, the effect of pressure on molecule orientation is negligible, regardless of the pore size.

Comparing the results for pore sizes of 0.49 and 0.61 nm, the relationship between filling up mechanism and molecular orientation can be observed. Thus for pores of 0.49 nm (Fig. 7(a)–(b)) molecules are clearly arranged in one layer for the entire pressure range, as shown by the evolution of the centre of mass profile. As pressure increases, the averaged angle of molecules also increases (up to around 40°), because the molecules are partially attracted by both pore walls at once. As the pore is filled up there is no further change in molecular ordering. For pores of 0.61 nm (Fig. 7(c)), as the pore is filled up, a greater variation in the angle value is observed (from 40° to 50° aprox) as the result of a more significant molecule re-ordering. With respect to the centre of mass profile, at the lowest pressure of 2 kPa a plateau is observed (Fig. 7(d)), being negligible the density differences across the pore width. In addition, the angle distribution for the lower pressures (2 and 7 kPa) is practically equal (Fig. 7(c)). As pressure increases the beginning of a two peak density profile is observed. The angle distributions for these higher pressures show an increase in the middle region of the pore size, as the result of the molecules interacting at once with the pre-formed layers on each pore wall, as observed in Fig. 7(d). Condensation in the middle of the pore is not attained, due to a lack of pore volume, and to the high intensity of wall potential field in this narrow pore.

Observing the results for pores of 0.73 nm (Fig. 7(e)–(f)) a two-peak centre of mass profile is observed almost from the lowest pressure (Fig. 7(f)) and no angle variation with pressure is observed for molecules arranged in the two layers next to the pore walls (Fig. 7(e)). As pressure increases, there is a larger dispersion of angle values for molecules out of the two adsorbed layers. Density values, for this out-of-layer region, apparently decreases with pressure, probably due to a larger interaction of the molecules in the pre-formed layer. The results observed suggest that the pore filling mechanism is based on the parallel preferential molecular orientation close to the pore walls, and on the increase in molecular disorder within the pore middle region.

Finally, when the pore volume is enough to hold three molecule layers (Fig. 7(g)–(h)), the mechanism of pore filling becomes more dependent on pressure. Thus, for pressures below 50 kPa, the third layer is not formed yet (Fig. 7(h)) and there is no difference in angle distribution for those molecules out of the two layers close to the pore walls. As pressure increases up to 500 kPa, an incipient third layer of molecules appears in the middle of the pore (Fig. 7(h)), that also have a smaller angle distribution compared to molecules allocated between the three parallel layers (Fig. 7(g)). This tendency is more pronounced for higher pressure values.

These results suggest that molecule orientation for molecules allocated in the out-of-layer region is the result of fluid interaction with molecules arranged in the three parallel layers.

5 Conclusion

Adsorption of a supercritical linear-molecule gas, like ethane, in slit shaped micropores slightly differing in their size has been studied. Sequential layer filling mechanism can be observed by considering the effect of pore width and pressure on the density profile and angle distribution of molecules across the pore size.

Adsorbate density attained in each pore size shows an oscillation shape as pore size is increased due to differences in packing efficiency. This efficiency is related to the number of adsorbate layers that can form within the pore volume. As pore width increases, for the pore size range containing only one adsorbate layer, molecule-wall angle also increases, revealing a larger molecule disorder that is related to a loss of adsorption capacity, as observed in the simulated adsorption isotherms. For the pore size range holding two adsorbate layers, the tendency is the opposite up to a pore size of 0.73 nm, where the two adsorbate layers are clearly different. A further decrease in adsorption capacity is observed until the third layer is attained. In the transition from two to three adsorbed layers, as pore size increases, a molecular reorientation is observed just before pore size is large enough to hold three layers.

The dependency of molecule packing efficiency on pressure can be observed by following the filling up mechanism in terms of density and angle distribution. Pressure effect is more remarkable for pore sizes exhibiting some condensation. Thus, fluid-fluid interactions between the various adsorbed layers are determinant revealing a vertical molecular orientation within these regions.

As a qualitative observation, pore sizes where molecular packing is less effective are characterized by

a greater molecular disorder, and consequently show a smaller adsorption capacity. These pore sizes may be present in many adsorbents and their contribution to total adsorption isotherm should be less important than the remaining pore sizes.

References

Allen, M.P. and D.J. Tildesley, *Computer Simulation of Liquids*, Oxford University Press, Oxford (1989).

Cracknell, R.F. and D. Nicholson, "Grand Canonical Monte Carlo Study of Lennard-Jones Mixtures in Slit Pores–part 3," *J. Chem. Soc. Faraday Trans.*, **90**, 1487 (1994).

Davies, G.H. and N.A. Seaton, "Predicting Adsorption Equilibrium Using Molecular Simulation," *AIChE J.*, **46**, 1753 (2000).

Do, D.D. and H.D. Do, "Adsorption of Ethylene on Graphitized Thermal Carbon Black and in Slit Pores: A Computer Simulation Study," *Langmuir*, **20**, 7103 (2004).

Duque, D. and L.F. Vega, "Some Issues on the Calculation of Interfacial Properties by Molecular Simulation," *J. Chem. Phys.*, **121**, 8611 (2004).

Frenkel, D. and B. Smit, *Understanding Molecular Simulation from Algorithms to Applications*, Academic Press, London (2002).

Gall, G.H. and E.S. Sanders, "Membrane Technology Removes CO_2 from Liquid Ethane," *Oil & Gas Journal*, **100**, 48 (2002).

Klochko, A.V., E.N. Brodskaya, and E.M. Piotrovskaya, "Computer Simulation of Dependence of Adsoprtion Characteristics of Ethane on the Size of Graphite Micropores," *Langmuir*, **15**, 545 (1999).

Lachet, V., A. Boutin, B. Tavitian, and A.H. Fuchs, "Grand Canonical Monte Carlo Simulations of Adsorption of Mixtures of Xylene Molecules in Faujasite Zeolites," *Faraday Discuss*. **106**, 307 (1997).

Liu, J.-C. and P.A. Monson, "Molecular Modeling of Adsorption in Activated Carbon: Comparison of Monte Carlo Simulation with Experiment," *Adsorption*, **11**, 5 (2005).

Lozano-Castelló, D., J. Alcañiz-Monge, M.A. de la Casa-Lillo, D. Cazorla Amorós, and A. Linares-Solano, "Review: Advances in the Study of Methane Storage in Porous Carbonaceous Materials," *Fuel*, **81**, 1777 (2002).

Martin, M.G. and J.I. Siepmann, "Transferable Potentials for Phase Equilibria. 1. United-Atom Description of *n*-Alkanes," *J. Phys. Chem. B*, **102**, 2596 (1998).

McQuarrie, D.A. and J.D. Simon, *Physical Chemistry: A Molecular Approach*, University Science Books, Sausalito, 1997.

Mota, J.B. "Impact of Gas Composition on Natural Gas Storage by Adsorption," *AIChE J.*, **45**, 986 (1999).

Neimark, A.V. and P.I. Ravikovitch, "Calibration of Pore Volume in Adsorption Experiments and Theoretical Models," *Langmuir*, **13**, 5148 (1997).

Nguyen, T.X., S.K. Bhatia, and D. Nicholson, "Packing Transitions of Lennard Jones Fluids in Carbon Slit Pores," *Annales Universitatis Mariae Curie-Sklodowoska*, **57**, 158 (2002).

Olivier, J.P. "Improving the Models Used for Calculating the Size Distribution of Micropore Volume of Activated Carbon from Adsorption Data," *Carbon*, **36**, 1469 (1998).

Poling, B.E., J.M. Prausnitz, and J.P. O'Connell, *The Properties of Gasses and Liquids*, Mc Graw Hill, New York (2001).

Steele, W.A. *The Interaction of Gases with Solids Surfaces*, Pergamon Press, Oxford (1974).

Suzuki, T., K. Kaneko, and K.E. Gubbins, "Pore Width-Sensitive Filling Mechanism for CCl_4 in a Graphitic Micropore by Computer Simulation," *Langmuir,* **13**, 2545 (1997).

Vishnyakov, A., E.M. Piotrovskaya, and E.N. Brodskaya, "Monte Carlo Computer Simulation of Adsorption of Diatomic Fluids in Slit-like Pores," *Langmuir*, **12**, 3643 (1996).

Yan, B. and X. Yang, "Adsorption Prediction for Three Binary Supercritical Gas Mixtures on Activated Carbon Based on a NDFT/PSD Approach,"*Chemical Eng. Sci.*, **60**, 3267 (2005).

Zhou, L., J. Wu, M. Li, Q. Wu, and Y. Zhou, "Prediction of Multicomponent Adsorption Equilibrium of Gas Mixtures Including Supercritical Components," *Chemical. Eng. Sci.*, **60**, 2833 (2005).